

Estimation of Rainfall and its Error Characteristics from Satellite Observations

Peter Bauer, ECMWF

Jean-François Mahfouf, Meteorological Service of Canada

GEWEX Workshop on Objective Analysis of Precipitation, ECMWF, 11-13 March 2003

1. Introduction

Currently, rainfall retrieval over ocean from passive microwave satellite observations represents the best compromise between estimation accuracy and spatial data coverage. Infrared data is available with higher temporal frequency from geostationary satellites but the link of top-of-the-atmosphere infrared emission to near-surface rainfall is very indirect. Therefore, all algorithms have to exploit the space-time relation between cloud cover / cloud top height and areal mean rainfall. With TRMM¹ the first spaceborne precipitation radar became available and provides the most detailed information on precipitation vertical structure and quantity over both land and ocean up to date.

The accuracy of precipitation estimates from satellite observations has been the target of numerous intercomparison studies (Ebert and Manton 1998, Smith et al. 1998, Adler et al. 2001) which were initiated to evaluate the large number of algorithms that had emerged with the availability of the operational SSM/I² series. As a consequence, permanent and globally coordinated activities have been founded such as the GPCP³, the TRMM validation field campaigns, and the WMO-IPWG⁴.

TRMM has also encouraged several data assimilation efforts (e.g. Marécal and Mahfouf 2002, Hou et al. 2002). In data assimilation, the proper definition of errors associated with the assimilated product is crucial because it determines the weight that is put on the observation in the analysis. Thus recent algorithm development efforts have made the error definition one of their key issues (Kummerow et al. 2001).

This paper presents two approaches for the estimation of rainfall retrieval errors as well as an example of the influence of data with different error characteristics on data assimilation. The latter is particularly important if, for example, data coverage has to be traded-off against data quality which becomes an issue in the preparation of GPM⁵. In this paper, retrieval errors are calculated using the definition of random errors inherent to the retrieval method itself and by the validation of retrieved profiles with independent data. Secondly, the issue of data quality/coverage in data assimilation is illustrated by comparing rainfall retrievals from TMI⁶ vs. SSM/I data in an assimilation experiment over one month.

2. Retrieval algorithm

Methodology

Bayes' formulation of the 'a posteriori' probability, $P(\mathbf{x}|\mathbf{y})$, that state \mathbf{x} occurs and observation \mathbf{y} can be made for non-linear problem is:

$$-2 \ln P(\mathbf{x} | \mathbf{y}) = [\mathbf{y} - \mathbf{F}(\mathbf{x})]^T \mathbf{S}_e^{-1} [\mathbf{y} - \mathbf{F}(\mathbf{x})] + [\mathbf{x} - \mathbf{x}_a]^T \mathbf{S}_a^{-1} [\mathbf{x} - \mathbf{x}_a] \quad (1)$$

¹ Tropical Rainfall Measuring Mission.

² Special Sensor Microwave / Imager.

³ Global Precipitation Climatology Project.

⁴ World Meteorological Organisation - International Precipitation Working Group.

⁵ Global Precipitation Mission.

⁶ TRMM Microwave Imager.

(e.g. Rodgers 2000). $\mathbf{F}(\mathbf{x})$ denotes the simulated observation with observation operator \mathbf{F} applied to state \mathbf{x} , and \mathbf{S} denotes the error covariance matrix of observation/simulation (index 'e') and 'a priori' state (index 'a'). Eq. (1) assumes that some 'a priori' knowledge exists and that the errors have Gaussian distributions. In the presence of clouds and precipitation the probability distribution $P(\mathbf{x}|\mathbf{y})$ is not very well described by a Gaussian distribution and the 'a priori' knowledge is difficult to obtain in a stand-alone algorithm so that the 'expected' value of $E(\mathbf{x})$ may be taken as a solution to the optimum estimate of \mathbf{x} that is the mean state averaged over the probability distribution:

$$E(\mathbf{x}) = \int \dots \int \mathbf{x} P(\mathbf{x} | \mathbf{y}) d\mathbf{x} \quad (2)$$

Using Eq. (1) and assuming that the two terms on the right hand side are uncorrelated:

$$E(\mathbf{x}) = \int \dots \int \mathbf{x} \exp\left\{-\frac{1}{2}[\mathbf{y} - \mathbf{F}(\mathbf{x})]^T \mathbf{S}_e^{-1}[\mathbf{y} - \mathbf{F}(\mathbf{x})]\right\} P(\mathbf{x}) d\mathbf{x} \quad (3)$$

$P(\mathbf{x})$ is the known distribution of $\mathbf{x}-\mathbf{x}_a$. Assuming that a database - say from combined cloud-radiative transfer model simulations - exists that represents sufficiently well the true distribution of \mathbf{x} , the integral may be replaced by a summation over all \mathbf{x}_i contained in the database:

$$E(\mathbf{x}) = A^{-1} \sum_i \mathbf{x}_i \exp\left\{-\frac{1}{2}[\mathbf{y} - \mathbf{F}(\mathbf{x}_i)]^T \mathbf{S}_e^{-1}[\mathbf{y} - \mathbf{F}(\mathbf{x}_i)]\right\} \quad (4)$$

with normalization factor:

$$A = \sum_i \exp\left\{-\frac{1}{2}[\mathbf{y} - \mathbf{F}(\mathbf{x}_i)]^T \mathbf{S}_e^{-1}[\mathbf{y} - \mathbf{F}(\mathbf{x}_i)]\right\} \quad (5)$$

This form is used in several algorithms for the retrieval of precipitation from passive microwave observations (e.g. Kummerow et al. 1996, Olson et al. 1996, Bauer et al. 2001).

Error estimation

In a similar way, the retrieval uncertainty can be estimated:

$$E(\mathbf{x}') = E\left\{\left[\mathbf{x} - E(\mathbf{x})\right]\left[\mathbf{x} - E(\mathbf{x})\right]^T\right\} \quad (6)$$

Apart from numerous studies on algorithm validation by independent observations from rain gauges or surface radars, only a few have dealt with the error estimation from error modelling. Physical algorithm development usually involves the combined modelling of clouds, precipitation, and radiative transfer also accounting for effects such as radiometer viewing geometry and varying spatial resolution per channel. Therefore error modelling requires the estimation of individual error sources and their propagation through the entire modelling chain. At present, only this combined error has been analyzed in terms of contributions from signal ambiguity to the total error (Bauer 2001) or the insufficient representation of the natural variability in the retrieval database vs. modelling errors (L'Ecuyer and Stephens 2002).

Both Bauer et al. (2002) and L'Ecuyer and Stephens (2002) have quantified the gross functional dependence of rainfall retrieval errors as a function of rain rate on the basis of Eq. (6) and different datasets for algorithm training and application. Figure 1 shows this dependence for three different algorithms (PATER, BAMPR, 2A12 V5.1) which employ Eq. (4) but use different simulation databases and quality control checks. The solid lines represent the standard deviation between radiometer and precipitation radar (PR) estimates and the comparison suggests that the errors represented by Eq. (6) are quite realistic even though they only cover the random error component.

All algorithms have in common that the relative errors are fairly large at low rain rates (100-200%) because of the increasing noise contribution from surface emission and atmospheric/cloud background emission. In the region of highest sensitivity of microwave window channels with respect to precipitation (~1-20 mm/h), errors decrease to 50% or even less. Depending on whether the algorithm uses

higher frequency channels (Figure 1b, c) and the representativeness of the database, relative errors may increase again for larger rain amounts.

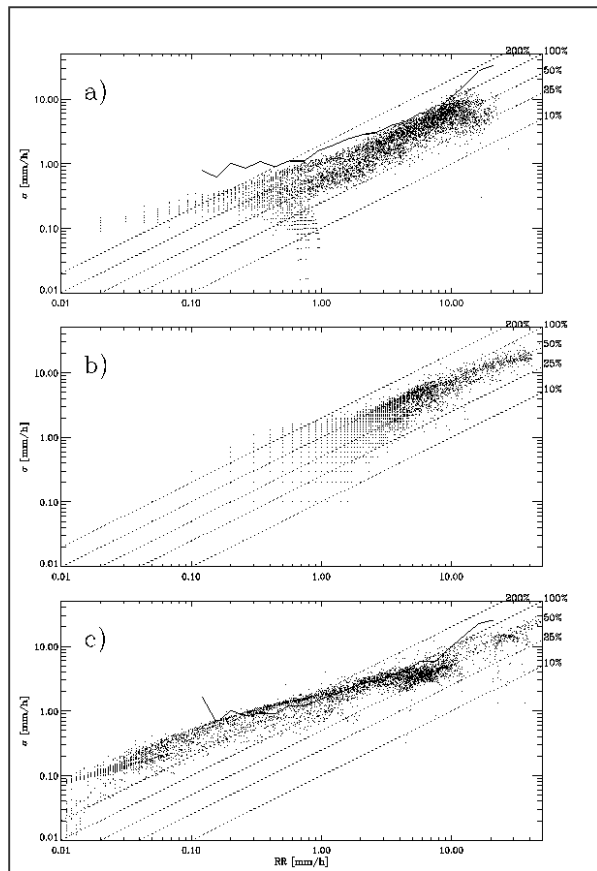
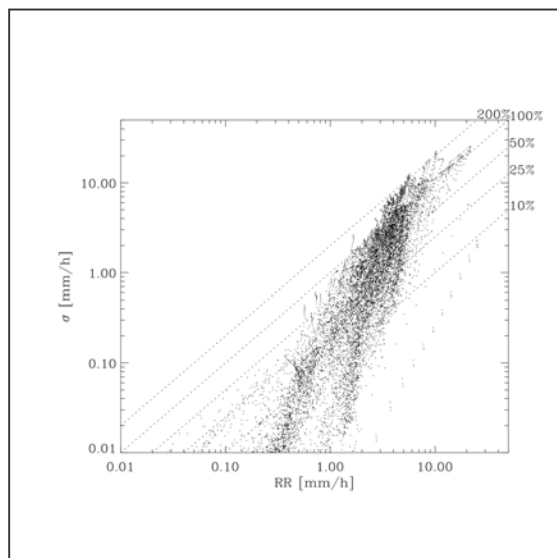


Figure 1: Bayesian retrieval errors from as a function of rain rate at product resolution for PATER (a), BAMPR (b), and 2A12 V5.1 (c). Superimposed are lines denoting average differences between PATER and PR (a) and 2A12 V5.1 and PR (c) retrievals, respectively [for algorithm details see Bauer et al. (2002)].

Application example

The retrieval algorithm [Eq. (4)] was implemented to demonstrate the potential of microwave temperature-sounding channels for precipitation profile retrieval. The algorithm uses a database from combined cloud-radiative transfer model simulations of hurricane Bonnie over the Western Carribean Sea. The cyclone was also well observed during the field campaign CAMEX-3⁷ on August 26, 1998. The retrieval method was applied to airborne observations with the NAST-M⁸ radiometer onboard the ER-2 aircraft. This radiometer has sounding channels in two oxygen absorption complexes near 50-57 GHz and 118.75 GHz (Blackwell et al. 2001). The channels in both bands are collocated in such a way that for a channel near 50 GHz there is a channel near 118 GHz with a similar clear-sky weighting function. Clouds and precipitation can

be sensed by their differential absorption and scattering features in both bands. Once precipitation profiles are retrieved, radar reflectivities can be simulated and compared to EDOP⁹ observations from the same aircraft. Therefore the retrieval accuracy can be estimated from the theoretical retrieval error given by Eq. (6) and by a comparison with radar reflectivities (Bauer and Mugnai 2003). The latter also leads to an estimate of systematic errors.



Several overpasses over hurricane Bonnie were carried out by the NASA ER-2 aircraft on August 26. The payload of the ER-2 aircraft also contained the ER-2 Doppler (EDOP) radar (Heymsfield et al. 1996). The EDOP radar is a two-antenna 9.6 GHz Doppler radar with one antenna pointing in nadir direction and the other pointing forward. In this study only the reflectivities from the nadir beam are used for validating the retrievals from NAST-M nadir observations.

Figure 2: Retrieval errors as a function of rain rates from aircraft data (> 200 000 data points).

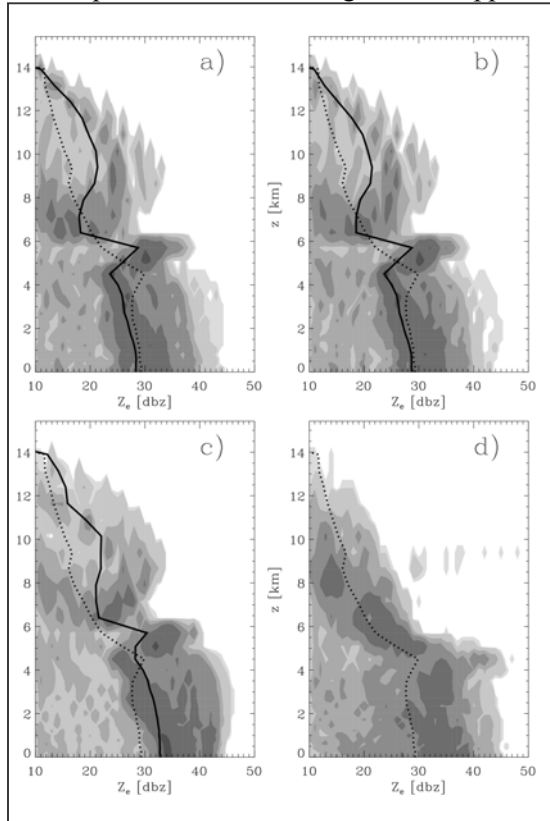
⁷ Convection and Moisture Experiment.

⁸ National Polar-Orbiting Operational Environmental Satellite System (NPOESS) Aircraft Sounder Testbed-Microwave (NAST-M).

⁹ ER-2 Doppler radar

A graph similar to Figure 1 was produced from the aircraft retrievals (Figure 2). While for rain rates > 5 mm/h, the errors match those from the satellite retrievals fairly well, the errors are much smaller below 5 mm/h. A possible explanation is the difference of spatial resolutions. This is because the aircraft data resolves details at 2 km scales while the satellite retrievals suffer from beam-filling errors that is the mismatch between spatially averaged high-resolution retrievals and retrievals from spatially averaged observations.

The retrieved profiles are converted to synthetic radar reflectivity profiles to be compared to the observed profiles. The advantage of this approach over the comparison of rain rates is that the utilization



of a radar retrieval algorithm with different assumptions on particle size distributions and optical properties is avoided. The comparison of reflectivities employs the same radiative transfer model that was used for the generation of the retrieval database. Therefore, attenuated reflectivities at any given frequency can easily be calculated and compared to the observations. The microwave retrievals were carried out for 2, 8, and 16 channels (at 50-57 and at 118 GHz) to test the contribution of channel combinations to retrieval accuracy, respectively.

The reflectivity statistics over all 929 profiles are summarized in Figure 3. The shading indicates the histograms of reflectivities vs. altitude and the solid lines represent the average profiles to be compared to the averaged observations given by the dashed line. The main observations are that both 16-channel and 8-channel retrievals work well and produce almost identical results. In the rain layer, average reflectivities agree within 1 dBZ (15-20% of rainrate).

Figure 3: Modelled EDOP reflectivity from NAST-M retrievals using 16 channels (a), 8 channels (b), 2 channels (c) as well as observed reflectivities (d).

Near the freezing level, differences occur for two reasons: (1) the observed freezing level height is near 5-5.5 km and the maximum of the bright band is at 4.5 km. The retrievals show a little more intense peak and a higher frequency of occurrence as well as a freezing level at 6.5 km.

This difference in altitude is explained by a temperature bias that was identified comparing (1) the temperature profiles from the database with those from the ECMWF analysis on 26/08/1998 at 12 UTC; (2) the clear-sky TB's between observations and simulations. Even though the biases in TB's may be corrected, the database still contains biased temperature profiles. Another observation is that the simulated reflectivities above freezing level are considerably higher (up to 5 dBZ) than the observed ones. This can only be explained by rather large differences between simulated and observed snow/graupel contents. In any case, the retrieval of rain profiles is not drastically affected by this problem.

3. Data assimilation of satellite derived rain rates

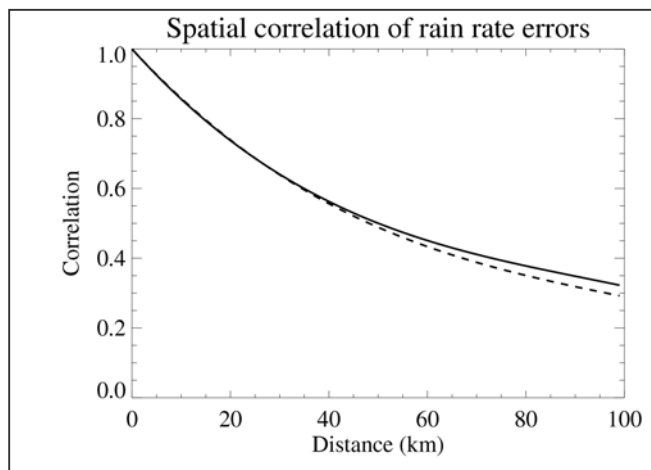
Rain rate retrievals from the microwave radiometers SSM/I and TMI have been calculated at pixel resolution and calibrated with data from the precipitation radar (PR) for TMI and SSM/I (Bauer et al. 2001). Each rain rate R_i (actually a rain liquid water content) is provided along with its error estimate. Averaged rain rates have been obtained by binning each observation within model grid boxes to avoid a spatial interpolation of temperature and humidity profiles at observation locations (Marécal and Mahfouf 2000). The estimation of averaged rain rate errors needs depends on their spatial correlation within each model grid box. The standard deviation of the mean rain rate is defined by:

$$\sigma_{\bar{R}} = \frac{1}{N} \left[\sum_{i=1}^N C_{ij} \sigma_i \sigma_j \right]^{1/2} \quad (7)$$

where C_{ij} is the spatial correlation of errors between two points i and j separated by a distance d_{ij} . Therefore, before computing rain rate averages and their associated errors, it is first necessary to use a sample of the raw satellite retrievals in order to compute C_{ij} .

On a model grid having a resolution of about 120 km, all pairs of rainy points within each model grid box were collected together with their associated errors. The use of a coarser grid than the actual model grid allows the computation of correlations over distances up to 120 km. The resolution of the TMI product is about 15 km with a sampling at ~ 10 km. Distances have been binned into 5 km intervals for TMI to compute spatial correlations. For SSM/I this distance is reduced to 25 km because this satellite has a coarser sampling. The polynomial fit used in Bauer et al. (2002) has been kept (with different coefficients):

$$C(r) = \sum_{k=0}^2 a_k r^k \quad (7)$$



The curves $C(r)$ are plotted in Figure 4 for TMI and SSM/I. The spatial correlations are very consistent between the two retrievals, since both TMI and SSM/I retrievals were calibrated with PR data. For a given 6-hour period (26 May 2002: 0300-0900 UTC) the TMI and SSM/I rain rates are plotted with their associated errors both at the pixel resolution (15 km for TMI and 25 km for SSM/I) and averaged to the model resolution (Figure 5).

Figure 4: Spatial correlation of TMI (solid line) and SSM/I (dashed line) rainfall rate retrieval errors.

At pixel resolution, important differences are noticed between the products. First, the lack of the 10 GHz channel and also the larger pixels reduce the SSM/I rain rate intensities to maximum values around 15 mm/h. On the contrary, the TMI product shows significant amounts of rain rates above 10 mm/h. The averaging procedure reduces error by 20-50%.

Ambiguities in the retrieval database are illustrated by the fact that some rain rate values can be retrieved with a wide range of different accuracies. For SSM/I rain rates, the larger footprint reduces the differences between the scatter plots at pixel and model resolution. Rain rate errors are usually larger than with TMI and there is a non-negligible amount of very low rain rates (< 0.01 mm/h) that may come from the different rejection criteria between the two products. However, it is unlikely that such small amounts could have a significant impact when assimilated due to the very large corresponding errors at model scale ($> 1000\%$). It is interesting to note that in the range 0.1 to 5 mm/h (peak of the model pdf) the errors between the two products are quite similar.

A series of three 4D-Var assimilation experiments starting on the 01 May 2001 over one month were performed using the ECMWF forecasting system. An ensemble of 10-day forecasts was also run from the 1200 UTC analyses. The assimilation system is an incremental 4D-Var where the minimisation is performed at a lower model resolution (horizontal grid about 120 km) and the assimilation window is 12 hours.

First, simplified 1D-Var assimilations of rain rates are performed every 6 hours using observations 3 hours before and after the analysis time to produce total column water vapour (TCWV) retrievals. Then these two batches of TCWV retrievals in rainy areas are introduced in 4D-Var as new observa-

tions. The first assimilation is a 'control' using the operational configuration of the forecasting system at the time, the second assimilation includes TMI PATER rain rates on top of all data from the control, while the third experiment is similar to TMI PATER but assimilates rain rates from SSM/I instead (two satellites are used: DMSP F-13 and F-14).

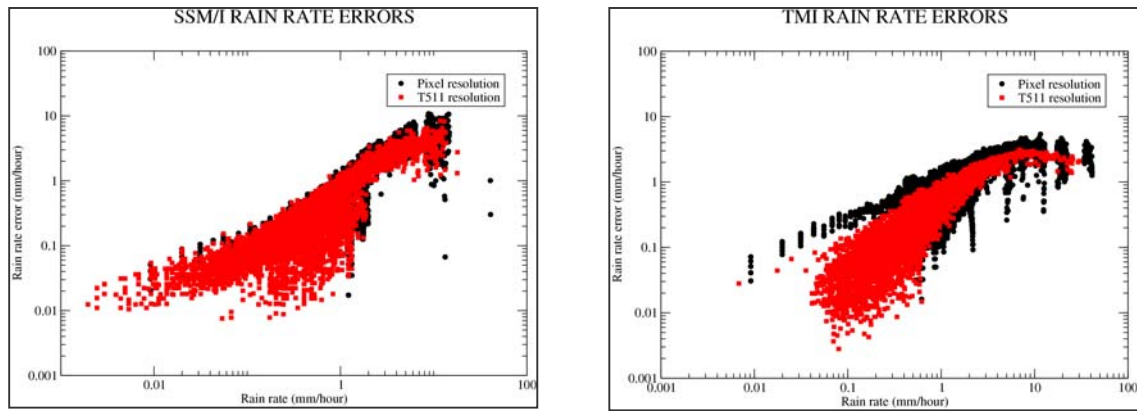


Figure 5: Errors as a function of rain rate at pixel resolution and model resolution (~40 km) for SSM/I products (left panel) and TMI products (right panel).

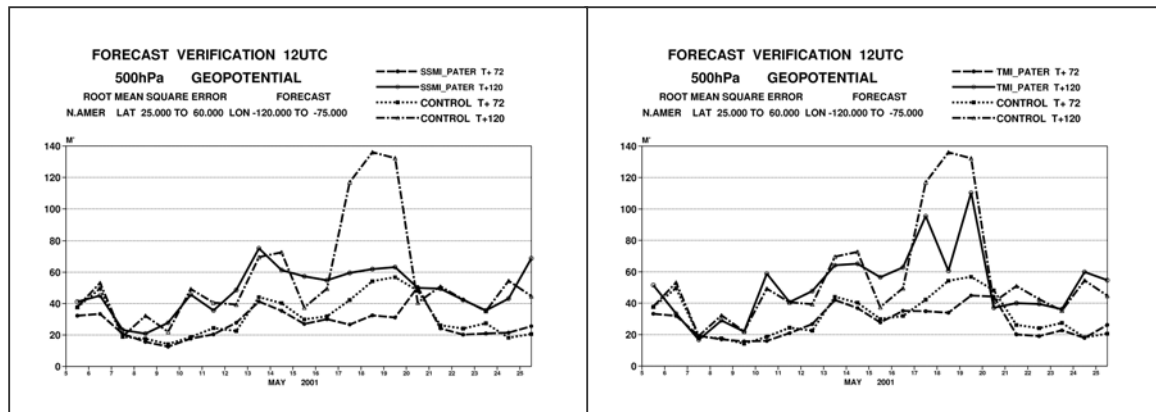


Figure 6: Time series (5-25 May 2001) of RMS errors of the geopotential at 500 hpa over North America for day-3 and day-5 forecasts issued from the control assimilation and from the assimilation with SSM/I (left) and TMI (right) derived rain rates.

Figure 6 shows time series of day-3 and day-5 forecasts for a 3-week period over the Northern American continent for the geopotential at 500 hpa. For three forecasts starting on the 17, 18 and 19 May the root mean square errors (rmse) at day-5 are larger than 100m. The impact of TMI data is to improve significantly the forecast starting on 2002/05/18 (rmse around 60m) and also to have a positive (but weaker) impact on the two other poor forecasts. The impact in the medium range is also present at shorter ranges (over this period there is an almost systematic improvement at 72 h). The impact of SSM/I data is even more spectacular since the three poor forecasts are all improved with rmse's reduced by more than a factor of two.

To the question: Is it better to have a small number of accurate rain rate observations (i.e. from TMI) than to have more observations but with a reduced accuracy (i.e. from SSM/I)? The answer from the above example is that it seems more beneficial to increase the number of observations because: (1) The accuracy of SSM/I and TMI are similar in the range of 0.1 mm/h to 5 mm/h corresponding to the maximum of the rainfall distribution. (2) Rather accurate TMI high intensity rain rates (by using the 10 GHz channel) are probably not assimilated efficiently because the model physics at 40 km resolution can hardly produce instantaneous rain rates above 10 mm/h (therefore quality control will tend to reject such observations).

4. Conclusions

From the experience of ~20 years of rainfall retrieval algorithm development, the 'physical' approach that is the Bayesian retrieval methodology applied to pre-defined databases from combined cloud-radiative transfer modelling emerged as the most versatile technique. This is because it provides the largest detail on the microphysical precipitation structure and because it allows the calculation of theoretical retrieval errors.

Comparing the errors obtained from different algorithms very similar features can be observed; however, there may be large differences comparing retrievals from spaceborne and airborne data due to beam-filling issues. In any case, systematic errors seem to be comparably small compared to random errors - this is a conclusion from the analysis of both airborne and spaceborne data.

Once rainfall observations are assimilated, the spatial error correlation has to be taken into account because the observations must be averaged to represent the spatial model resolution. Rainfall rate assimilation experiments with the ECMWF modelling system have shown that apart from the positive impact of the data on analyses and forecasts, the accuracy of the observations has to be traded off against the data coverage. Depending on the case, better coverage may compensate reduced accuracy. This will be an important research issue for future assimilation studies as well as algorithm design.

5. References

- Adler, R.F., C. Kidd, G. Petty, M. Morrissey, and H.M. Goodman, 2001: Intercomparison of global precipitation products: The third Precipitation Intercomparison Project (PIP-3). *Bull. Amer. Met. Soc.*, **82**, 1377-1396.
- Bauer, P., 2001: Over-ocean rainfall retrieval from multi-sensor data of the Tropical Rainfall Measuring Mission (TRMM). Part I: Design and evaluation of inversion databases. *J. Atmos. Oceanic Technol.*, **18**, 1315-1330.
- Bauer, P., P. Amayenc, C.D. Kummerow, and E.A. Smith, 2001: Over-ocean rainfall retrieval from multisensor data of the Tropical Rainfall Measuring Mission. Part II: Algorithm implementation. *J. Atmos. Oceanic Technol.*, **18**, 315-330.
- Bauer, P., J.-F. Mahfouf, W.S. Olson, F.S. Marzano, S. Di Michele, A. Tassa, and A. Mugnai, 2002: Error analysis of TMI rainfall estimates over ocean for variational data assimilation. *Quart. J. Roy. Meteor. Soc.*, **128**, 2129-2144
- Bauer, P. and A. Mugnai, 2003: Precipitation profile retrievals using temperature-sounding microwave observations. *J. Geophys. Res.*, submitted.
- Blackwell, W.J., J.W. Barrett, F.W. Chen, R.V. Leslie, P.W. Rosenkranz, M.J. Schwartz, and D.H. Staelin, 2001: NPOESS Aircraft Sounder Testbed-Microwave (NAST-M): Instrument description and initial flight results. *IEEE Trans. Geosci. Remote Sens.*, **39**, 2444-2453.
- Ebert, E. and M. Manton, 1998: Performance of satellite rainfall estimation algorithms during TOGA-COARE. *J. Atmos. Sci.*, **55**, 1537-1557.
- Heymsfield, G.M., S. Bidwell, I.J. Caylor, S. Ameen, S. Nicholson, W. Bonyck, L. Miller, D. Vandemark, P. E. Racette, and L.R. Dod, 1996: The EDOP radar system on the high altitude NASA ER-2 aircraft. *J. Atmos. Oceanic Tech.*, **13**, 795-809.
- Hou, A.Y., S. Zhang, and O. Reale, 2002: Variational continuous assimilation of TMI and SSM/I rainrates: Impact on GEOS-3 hurricane analyses and forecasts. *Mon. Wea. Rev.*, submitted.
- Kummerow, C.D., W.S. Olson, and L. Giglio, 1996: A simplified scheme for obtaining precipitation and vertical hydrometeor profiles from passive microwave sensors. *IEEE Trans. Geosci. Remote Sens.*, **34**, 1213-1232.
- Kummerow, C.D., Y. Hong, W.S. Olson, S. Yang, R.F. Adler, J. McCollum, R.R. Ferraro, G.W. Petty, D.-B. Shin, and T.T. Wilheit, 2001: The evolution of the Goddard Profiling Algorithm (GPROF) for rainfall estimation from passive microwave sensors. *J. Appl. Meteor.*, **40**, 1801-1820.
- L'Ecuyer, Y.S. and G.L. Stephens, 2002: An uncertainty model for Bayesian Monte-Carlo retrieval algorithms: Application to the TRMM observing system. *Q. J. R. Meteor. Soc.*, **128**, 1713-1737.
- Marécal V. and J.-F. Mahfouf, 2000: Variational retrieval of temperature and humidity profiles from TRMM precipitation data. *Mon. Wea. Rev.*, **128**, 3853-3866
- Marécal V. and J.-F. Mahfouf, 2002: Four-dimensional variational assimilation of total column water vapour in rainy areas. *Mon. Wea. Rev.*, **130**, 43-58
- Olson, W., C.D. Kummerow, G. Heymsfield, and L. Giglio, 1996: A method for combined passive-active microwave retrievals of cloud and precipitation profiles. *J. Appl. Meteor.*, **35**, 1763-1789.
- Rodgers, C.D., 2000: Inverse methods for atmospheric sounding, Theory and Practice. Series on Atmospheric, Oceanic and Planetary Physics, Vol. 2. World Scientific, Singapore, New Jersey, London, Hong Kong, 238 pp.
- Smith, E. and co-authors, 1998: Results of WetNet PIP-2 project. *J. Atmos. Sci.*, **55**, 1483-1536.